Inorganic Chemistry

Article

pubs.acs.org/IC

# Structural Investigation of $(U_{0.7}Pu_{0.3})O_{2-x}$ Mixed Oxides

Jean-François Vigier,*[,†] Philippe M. Martin,[‡] Laura Martel,[†] Damien Prieur,[†] Andreas C. Scheinost,[§] and Joseph Somers[†]

[†]European Commission, Joint Research Centre (JRC), Institute for Transuranium Elements (ITU), Postfach 2340, 76125 Karlsruhe, Germany

[‡]CEA, DEN, Cadarache DEC/SESC, F-13108 St-Paul-Lez-Durance Cedex, France

[§]Helmholtz-Zentrum Dresden-Rossendorf, Institute of Resource Ecology, D-01314 Dresden, Germany

**ABSTRACT:** Uranium−plutonium mixed oxide containing 30% of plutonium is a candidate fuel for several fast neutron and accelerator driven reactor systems. In this work, a detailed structural investigation on sol−gel synthesized stoichiometric $U_{0.7}Pu_{0.3}O_{2.00}$ and substoichiometric $U_{0.7}Pu_{0.3}O_{2-x}$, using X-ray diffraction (XRD), oxygen 17 magic angle spinning nuclear magnetic resonance ($^{17}$O MAS NMR) and X-ray absorption spectroscopy is described. As observed by XRD, the stoichiometric $U_{0.7}Pu_{0.3}O_{2.00}$ is monophasic with a lattice parameter in good agreement with Vegard's law, while the substoichiometric $U_{0.7}Pu_{0.3}O_{2-x}$ material is biphasic. Solid solution ideality in terms of a random distribution of metal atoms is proven for $U_{0.7}Pu_{0.3}O_{2.00}$ with $^{17}$O MAS NMR. X-ray absorption near-edge structure (XANES) spectroscopy shows the presence of plutonium(III) in $U_{0.7}Pu_{0.3}O_{2-x}$. Extended X-ray absorption fine-structure (EXAFS) spectroscopy indicates a similar local structure around both cations, and comparison with XRD indicates a close similarity between uranium and plutonium local structures and the long-range ordering.

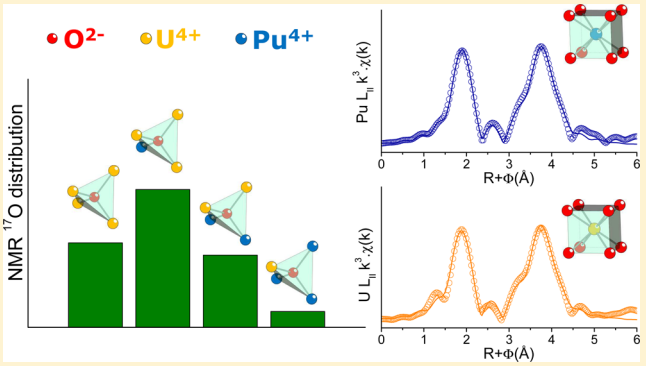


## INTRODUCTION

Uranium plutonium mixed oxide (MOX) fuel with low plutonium content ($PuO_2$ < 10%) is used as nuclear fuel in several thermal neutron reactors around the world. MOX with higher plutonium content is expected to be a favorable fuel for fast neutron reactors. The selected composition for the subcritical core design[1] of the accelerator driven system MYRRHA, currently in development, is 30% of $PuO_2$ (MOX30). A similar composition is also considered for other Generation IV fast reactors.[2] In this context, this study proposes a detailed structural characterization of MOX30, both on stoichiometric $U_{0.7}Pu_{0.3}O_{2.00}$ and on substoichiometric $U_{0.7}Pu_{0.3}O_{2-x}$ materials. The constraint of the O/M (M = U + Pu) ratio below 2.00 is chosen as a safety precaution to protect the steel cladding from corrosion during irradiation in fast neutron reactors, even though this substoichiometry has also negative consequences like a reduced thermal conductivity[3] or the biphasic composition of the MOX.

The long-range ordering of MOX fuels has been studied extensively by XRD. Stoichiometric MOX $U_{1-y}Pu_yO_{2.00}$ has a fluorite structure with a lattice parameter following Vegard's law for all range of composition ($0 \le y \le 1$).[4] In the case of substoichiometric MOX, a single fluorite structure is maintained for low plutonium contents ($y < 0.2$), while 2 phases are observed for higher plutonium contents ($y > 0.2$).[5] In the case of $U_{0.7}Pu_{0.3}O_{2-x}$, both phases exhibit fluorite structures, the first one with a O/M ratio close to 2.00, while the second has a lower oxygen content.

Data on the local structure are more limited. EXAFS and XANES spectra of MOX30 have been previously published,[6] but the material in this study was slightly overstoichiometric $U_{0.7}Pu_{0.3}O_{2+x}$. $^{17}$O MAS NMR has never been applied to characterize MOX.

The properties of stoichiometric $U_{0.7}Pu_{0.3}O_{2.00}$ are based on the assumption of an ideal solid solution, involving random distribution of Pu and U, and a similar local structure surrounding both cations. Therefore, we probed the short-range order around oxygen by using $^{17}$O MAS NMR spectroscopy, and around the two cations by using U-$L_{II}$ and Pu-$L_{II}$ edge EXAFS spectroscopy. Furthermore, the electronic properties were investigated by XANES spectroscopy at U-$L_{III}$ and Pu-$L_{III}$ edges.

For substoichiometric $U_{0.7}Pu_{0.3}O_{2-x}$, the material sensitivity to oxidation, recently studied by Vauchy,[7] will be described to rigorously compare XRD and EXAFS-XANES data. To our knowledge, this study provides the first published EXAFS-XANES results of substoichiometric MOX. In the recent data published on MOX melting point by Böhler et al.,[8] only XANES is performed, and substoichiometry is not clearly observed.

**Received:** February 18, 2015
**Published:** May 18, 2015

  

DOI: 10.1021/acs.inorgchem.5b00392
*Inorg. Chem.* 2015, 54, 5358−5365

## EXPERIMENTAL SECTION

**Synthesis.** The MOX powder was synthesized by gel-supported precipitation (also referred as sol–gel external gelation). This technique is known to give a homogeneous solid solution,[9] without any milling step before sintering, as necessary in powder metallurgy methods.[4] Uranyl nitrate was dissolved in water and $PuO_2$ in concentrated nitric acid (14 M). The solutions were then mixed in the desired ratios. An organic thickener (Methocel, Dow Chemicals) was added to increase the viscosity of the solution. The resulting solution was passed through a high speed rotating cup to obtain droplets, which were collected in an ammonia bath where actinide hydrolysis took place. The particles were dried and calcined at 700 °C under air and at 800 °C in Ar–4%$H_2$ to provide the dioxide feed powder. This powder was pressed into pellets and sintered at 1600 °C for 8 h. The atmosphere applied during sintering was Ar–4%$H_2$ for the substoichiometric $U_{0.7}Pu_{0.3}O_{2-x}$ sample, and Ar–4% $H_2$–2000 ppm $H_2O$ for the stoichiometric $U_{0.7}Pu_{0.3}O_{2.00}$ sample.[10] The isotopic composition of the material is detailed in Table 1.

**Table 1. Composition of MOX Used in This Study**[a]

| | isotope content | uncertainty | elemental content | uncertainty |
|---|---|---|---|---|
| $x(^{238}Pu)$ | 0.04% | ±0.01% | | |
| $x(^{239}Pu)$ | 22.17% | ±0.15% | | |
| $x(^{240}Pu)$ | 6.35% | ±0.08% | | |
| $x(^{241}Pu)$ | 0.22% | ±0.01% | | |
| $x(^{242}Pu)$ | 0.42% | ±0.08% | | |
| $x_{Pu}$ | | | 29.19% | ±0.32% |
| $x(^{241}Am)$ | 0.64% | ±0.01% | | |
| $x_{Am}$ | | | 0.64% | ±0.01% |
| $x_U$ | | | 70.17% | ±0.33% |
| total | | | 100.00% | |

[a]The values are in mol % relative to the total actinide content (uranium, plutonium, and americium).

For $^{17}O$ MAS NMR analysis, a sample of MOX powder was enriched before sintering. A $^{17}O$ enrichment of about 30% was obtained by heating in oxygen-17 enriched $O_2$ gas (Cortecnet, 70% oxygen-17 enriched) at 800 °C for 24 h. Then, the powder was sintered at 1600 °C (8 h) under Ar–4% $H_2$–2000 ppm $H_2O$ to obtain the stoichiometric $U_{0.7}Pu_{0.3}O_{2.00}$ composition.

**X-ray Diffraction.** XRD analyses were performed on crushed samples from pellets. About 20 mg of powder is loaded in an epoxy resin to avoid any dispersion. A Bruker D8 Advance diffractometer (Cu K$\alpha$ radiation, 40 kV, and 40 mA) with a Bragg–Brentano $\theta/2\theta$ configuration, implanted in a radioactive glovebox, was used for the analyses. This diffractometer was equipped with a curved Ge monochromator (111) and a Lynxeye linear position-sensitive detector. The powder patterns were recorded using a step size of 0.01° across the angular range $10° \leq 2\theta \leq 120°$. Structural analyses were performed by the Rietveld method using Jana2006 software.[11] Peak profile fitting was achieved using pseudo-Voigt functions.

**$^{17}O$ MAS NMR.** The NMR experiment was performed on a 9.4 T Bruker spectrometer at the Larmor frequency of 54.243 MHz. This equipment is combined with an active glovebox dedicated to the handling of radioactive materials, and described in detail elsewhere.[12] The rotor was spun at 50 kHz. The Hahn echo experiment was made with duration of 4 $\mu$s ($\pi/2$) and 8 $\mu$s ($\pi$). The spectrum was calibrated to 0 ppm relative to liquid $H_2O$ enriched in $^{17}O$ and fitted using the dmfit software.[13]

**EXAFS-XANES.** XANES and EXAFS measurements have been performed on approximately 1 mg of powdered sample mixed with 20 mg of boron nitride (BN). The data have been collected at the Rossendorf beamline (ROBL) at the European Synchrotron Radiation Facility (ESRF) situated in Grenoble (France), using a Si(111) double-crystal monochromator and two Rh-coated mirrors for collimation and suppression of higher harmonics.[14] Data were simultaneously collected in transmission and fluorescence modes at the $L_{II}$ and $L_{III}$ edges of U and Pu. Fluorescence signals were measured with a 13-element Ge solid state detector (Canberra) using a digital spectrometer (XIA-XMAP). Energy calibration of the monochromator was achieved by using Y (17 038 eV), Zr (17 998 eV), and Mo (20 000 eV) foils located between the second and the third ionization chamber. The $E_0$ values were taken at the first edge inflection point determined by the node of the second derivative.

To determine the oxidation states of the cations, XANES spectra at the $L_{III}$ edge were compared to data collected on reference compounds on the same beamline using the same experimental setup. For uranium, the reference compounds were $UO_{2.00}$ and $U_4O_9$. Their structures were confirmed using both XRD and neutron diffraction.[15]

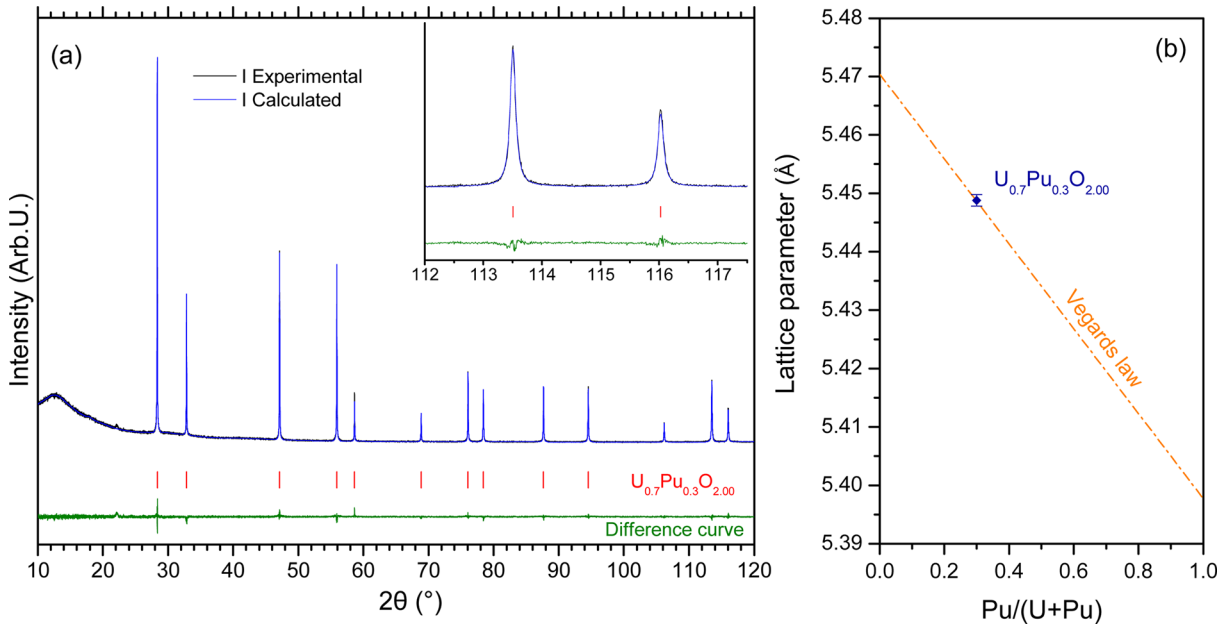


**Figure 1.** (a) XRD pattern of freshly sintered and crushed $U_{0.7}Pu_{0.3}O_{2.00}$ pellet sample ($R_p$ = 4.58%, $R_{wp}$ = 6.74%) and (b) comparison of the fitted $U_{0.7}Pu_{0.3}O_{2.00}$ lattice parameter with Vegard's law.



DOI: 10.1021/acs.inorgchem.5b00392
Inorg. Chem. 2015, 54, 5358–5365

For plutonium, the reference materials were $Pu^{+IV}O_{2.00}$[16] and $Pu^{+III}$ oxalate. The molar fractions of the cations were assessed using a linear combination of reference compounds from the normalized $\mu(E)$ spectra. Experimental data were fitted between −20 eV and +30 eV of the white line energy maximum.

The *ATHENA* software[17] was used to extract EXAFS oscillations from the raw absorption spectra. Curve fitting with the *ARTEMIS* software was performed in $k^3$ space. Experimental EXAFS spectra were Fourier-transformed using a Hanning window over the full $k$ range available at the respective edges. Phases and amplitudes for the interatomic scattering paths were calculated with the *ab initio* code FEFF8.40. Spherical atomic clusters with a radius of 8 Å based on the fluorite-type structure were used for the FEFF calculations. Each cation position in the cluster of atoms was filled with 50% of U and 50% of Pu. For each shell, the coordination numbers were fitted separately. Considering the negligible difference in the calculated amplitude and phase shifts, cation−cation shells were modeled using one metallic backscattering element. In addition to the three Me−O1 Me−Me and Me−O2 interatomic distances, the multiple scattering was also considered during shell fit using the multiple-scattering path (Me−O−Me−O−Me). As often employed for An $L_{III}/L_{II}$ investigations,[6,18−21] the amplitude factor ($S_0^2$) was set at 1.0 for U and Pu $L_{II}$ edges. The shift in the threshold energy ($\Delta E_0$) was varied as a global parameter.

## RESULTS AND DISCUSSION

**Characterization of Stoichiometric MOX.** The XRD pattern of $U_{0.7}Pu_{0.3}O_{2.00}$, presented in Figure 1, shows a single

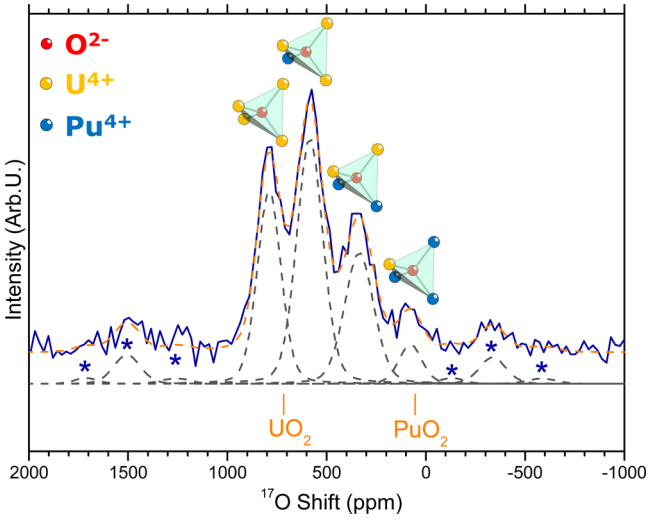


**Figure 2.** Experimental and fitted $^{17}O$ MAS NMR spectra (solid and dashed curves, respectively) of the $U_{0.7}Pu_{0.3}O_{2.00}$ sample acquired at 50 kHz. The stars indicate the spinning sidebands. The $^{17}O$ shifts for pure $UO_2$ and $PuO_2$ are shown.[25]

phase formed after the sintering process. Both the symmetry and the low full width at half maximum (FWHM) of the diffraction peaks, even at high angles, reveal good homogeneity and crystallinity of the material. The Rietveld refinement of the diffractogram gives a lattice parameter of 5.4488(9) Å. The excellent agreement of this value with Vegard's law is consistent with the formation of stoichiometric MOX $U_{0.7}Pu_{0.3}O_{2.00}$. Deviation from this tendency is observed, with lower values in the case of hyperstoichiometric compositions $U_{0.7}Pu_{0.3}O_{2+x}$[6] and higher values in the case of substoichiometric compositions $U_{0.7}Pu_{0.3}O_{2-x}$.[22] Furthermore, consistency with Vegard's law suggests the formation of an ideal solid solution. The ideality of such solid solutions has been proven by Martin et al.[18] on the

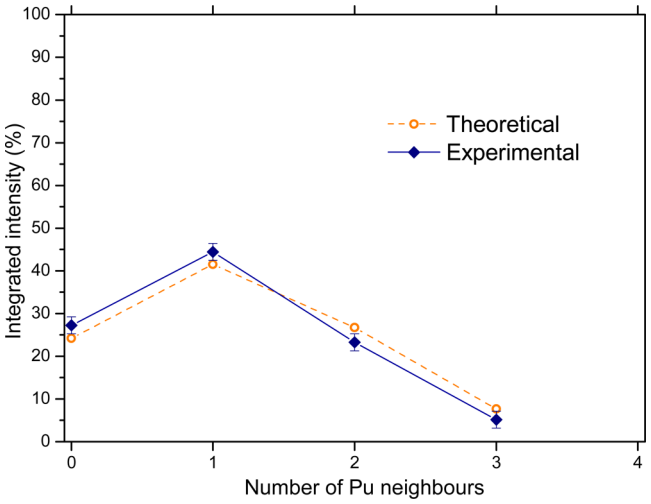


**Figure 3.** Plot of experimental and theoretical intensities with the number of Pu neighbors around the oxygen atoms. The theoretical intensities correspond to a randomly distributed network.

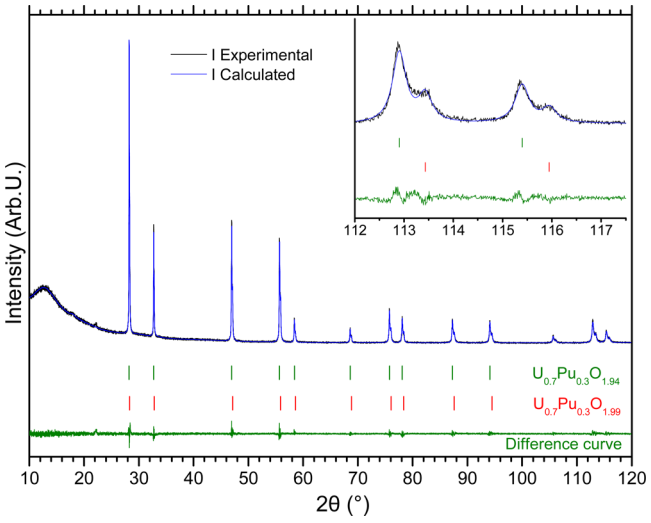


**Figure 4.** XRD pattern of freshly sintered and crushed $U_{0.7}Pu_{0.3}O_{2-x}$ pellet sample ($R_p$ = 4.87%, $R_{wp}$ = 7.08%).

MOX surrogate $(U_{1-x}Ce_x)O_{2.00}$ for different cationic composition using EXAFS. In that case, the uranium and cerium ratio present in the second cation shell can be deduced from EXAFS data and are experimentally consistent with a random distribution of uranium and cerium in the lattice. Unfortunately, the same procedure cannot be applied to $(U_{1-x}Pu_x)O_{2.00}$ as uranium and plutonium at the second shell cannot be distinguished in EXAFS due to their similar atomic numbers. More recently, $^{17}O$ MAS NMR has been successfully used to investigate the cationic distribution in $(U_{1-x}Np_x)O_{2.00}$ materials, for the full composition range.[23] The same method is applied for this study for the stoichiometric $U_{0.7}Pu_{0.3}O_{2.00}$. In the MOX fluorite structure, each oxygen atom is at the center of a cationic tetrahedron $O(U)_{4-z}(Pu)_z$ with 5 possible compositions due to solid solution ($0 \le z \le 4$). The $^{17}O$ MAS NMR spectrum presented in Figure 2 shows a specific signal for each uranium−plutonium environment $O(U)_{4-z}(Pu)_z$ ($0 \le z \le 3$). The integrated intensity of each signal is proportional to the quantity of oxygen atoms in each environment. Therefore, peak deconvolution gives the experimental oxygen site distribution


DOI: 10.1021/acs.inorgchem.5b00392
*Inorg. Chem.* 2015, 54, 5358−5365

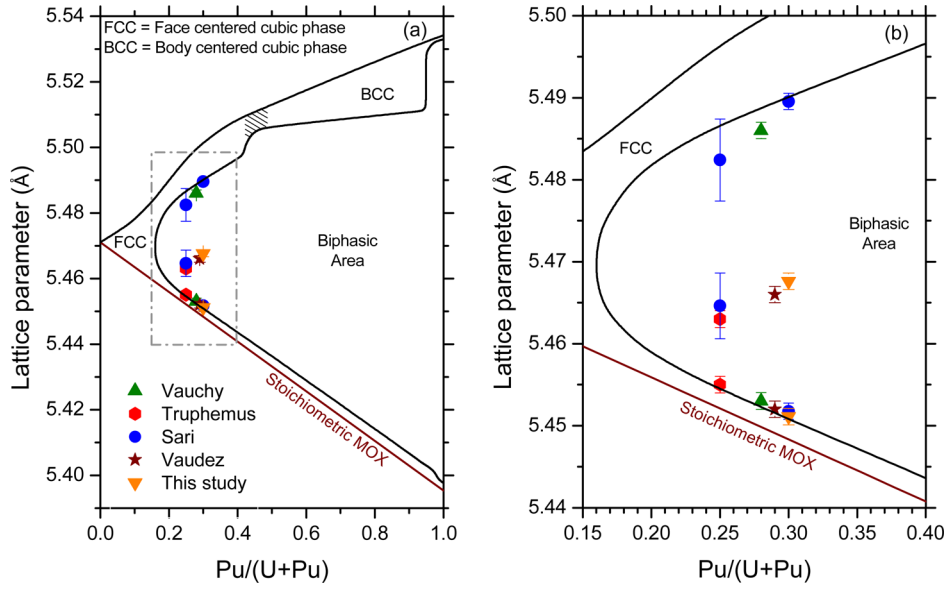


**Figure 5.** Experimental lattice parameters of the biphasic $U_{0.7}Pu_{0.3}O_{2-x}$ in comparison with the ternary system of Sari et al.[5] Other experimental values of biphasic $U_{1-y}Pu_yO_{2-x}$ in the same range of Pu content are also reported.[2,26,27] (a) Full phase diagram. (b) Expanded part of the phase diagram.

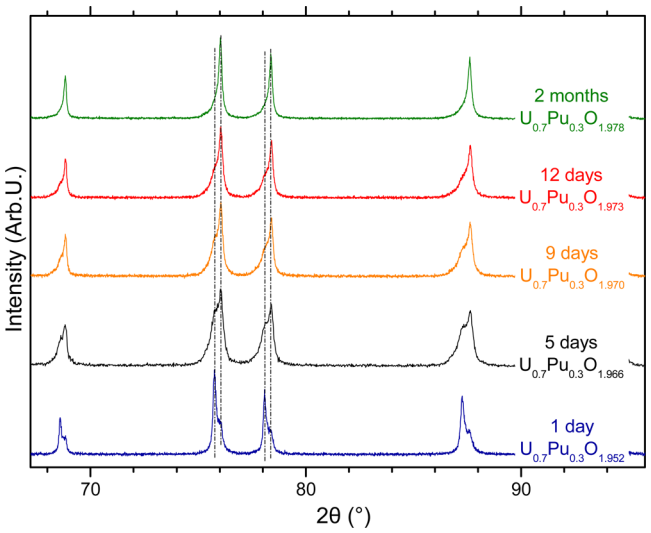


**Figure 6.** Evolution of the $U_{0.7}Pu_{0.3}O_{2-x}$ XRD pattern with time, showing the oxidation of the crushed sample. The average O/M ratios were deduced from Rietveld refinement. Atmosphere: $N_2 + O_2 \approx 0.6\% + H_2O \approx 7$ ppm.

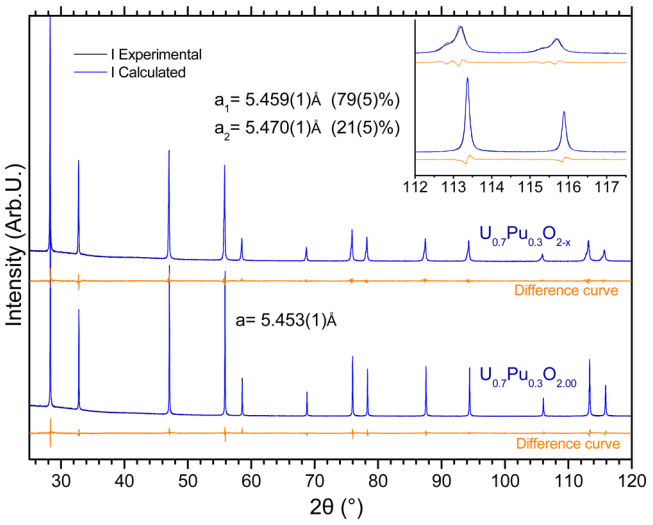


**Figure 7.** XRD pattern of $U_{0.7}Pu_{0.3}O_{2.00}$ ($R_p$ = 2.61%, $R_{wp}$ = 4.33%) and $U_{0.7}Pu_{0.3}O_{2-x}$ ($R_p$ = 2.66%, $R_{wp}$ = 4.23%), one year after sintering and one month after crushing for analysis (same as for the EXAFS-XANES experimental conditions). Lattice parameters and phase proportions are calculated by Rietveld refinement.

(Figure 3). No $O(Pu)_4$ entities are observed as their concentration (~0.8%) is too low for this composition and as the signal would overlap spinning sidebands. Good agreement between the values calculated for a random uranium–plutonium distribution model in an ideal solid solution and the experimental ones is found. From the structural point of view, this data gives strong evidence of the solid solution ideality for $U_{0.7}Pu_{0.3}O_{2.00}$ and the presence of cation clustering can be discarded.

The peak positions are detected at 789, 584, 336, and 77 ppm for $O(U)_4$, $O(U)_3(Pu)_1$, $O(U)_2(Pu)_2$, and $O(U)_1(Pu)_3$, respectively. A shift in the signal is observed for $O(U)_4$ entities between pure $UO_2$ (717 ppm) and $U_{0.7}Pu_{0.3}O_{2.00}$ (Figure 2). This phenomenon has been already observed in other materials when comparing pure compounds and solid solutions.[23,24]

**Characterization of Substoichiometric MOX.** The substoichiometric MOX $U_{0.7}Pu_{0.3}O_{2-x}$ sample presents a biphasic composition (Figure 4), in agreement with previously reported experimental data[2,5,26,27] and the thermodynamic model.[28] While $U_{0.7}Pu_{0.3}O_{2-x}$ is monophasic at high temperature during the sintering process, a phase separation occurs during the cooling step at relatively low temperature (*ca.* 600 K), driven by the oxygen mobility in the material and giving a mixture of high (close to stoichiometry) and low oxygen content MOX with the same uranium–plutonium ratio in both phases.[27] The deviation from stoichiometry in each phase can be deduced from the lattice parameter using the formula[29]

$$a(\text{pm}) = 547.0 - 7.4y + 32x \quad (1)$$

where $x$ and $y$ correspond to the general formula $(U_{1-y}Pu_y)O_{2-x}$.



DOI: 10.1021/acs.inorgchem.5b00392
*Inorg. Chem.* 2015, 54, 5358–5365

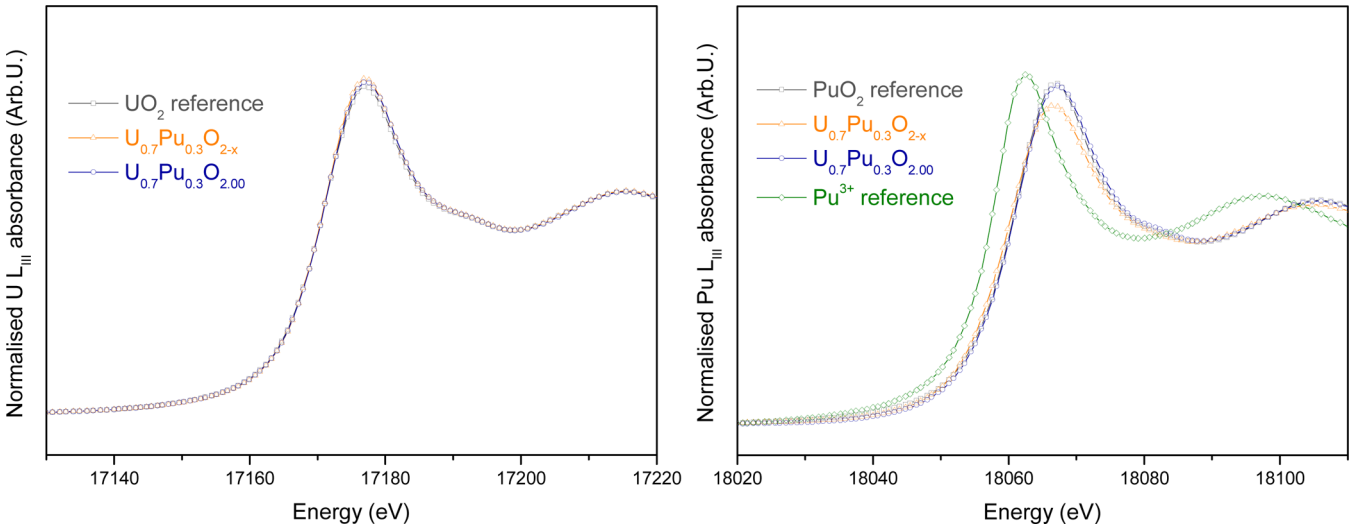


**Figure 8.** XANES spectra at U-$L_{III}$ and Pu-$L_{III}$ edges.

**Table 2. Molar Fraction of U(+IV), Pu(+III), and Pu(+IV) Deduced from a Linear Combination Fit of the XANES Spectra (1% Uncertainties)**

| | molar fraction (%) | | | | |
|---|---|---|---|---|---|
| | $U^{+IV}$ | $Pu^{+III}$ | $Pu^{+IV}$ | O/M | $R_{factor}$ Pu-$L_{III}$ |
| $U_{0.7}Pu_{0.3}O_{2.00}$ | 70 | 0 | 30 | 2.000 (10) | $3 \times 10^{-4}$ |
| $U_{0.7}Pu_{0.3}O_{2-x}$ | 70 | 4 | 26 | 1.978 (10) | $3 \times 10^{-4}$ |

The substoichiometric MOX obtained here corresponds to a mixture of 28(5)% of $U_{0.7}Pu_{0.3}O_{1.99}$ (5.4510(9) Å) and 72(5)% of $U_{0.7}Pu_{0.3}O_{1.94}$ (5.4676(9) Å). The phase proportion is deduced from Rietveld refinement, and corresponds to an overall composition of $U_{0.7}Pu_{0.3}O_{1.952}$. The lattice parameters are compared with values given for the ternary system by Sari et al.[5] in Figure 5. The experimental and predicted cell parameters for the phase close to stoichiometry (i.e., $U_{0.7}Pu_{0.3}O_{1.99}$) are in very good agreement, but the low oxygen content phase shows significant differences to the earlier study. Nevertheless, as illustrated by Figure 5, a significant discrepancy exists in the literature[2,5,26,27] concerning the lattice parameters in this plutonium composition range. The close proximity of the miscibility gap delimiting monophasic and biphasic substoichiometric MOX is probably responsible of these differences, with the separation itself very sensitive to experimental parameters (sintering conditions, actinide homogeneity, impurities content, etc.).

For the EXAFS analyses, samples are prepared with small quantities of powder from crushed pellets. Due to the radiation protection rules, sample preparation is generally performed several weeks before analysis at the synchrotron. For this reason, the oxidation sensitivity of substoichiometric MOX has to be considered. After crushing a sample of a sintered pellet for analysis, the material is exposed to the glovebox atmosphere. Despite the use of an inert atmosphere (nitrogen), a slow oxidation of the sample occurs. During this oxidation, a change of phase proportion is observed with a decrease of the low oxygen content phase $U_{0.7}Pu_{0.3}O_{1.94}$ and an increase of the $U_{0.7}Pu_{0.3}O_{1.99}$ phase (Figure 6). This room temperature oxidation has been studied recently by Vauchy.[7] His work has shown that the oxygen content in the nitrogen has no significant impact on the oxidation kinetics. In our study the oxygen content in the nitrogen was higher ($O_2 \approx 0.6\%$ and $H_2O \approx 7$ ppm vs $O_2 \approx 30$ ppm and $H_2O \approx 50$ ppm for Vauchy), but the material oxidation is significantly slower than that described by Vauchy (*ca.* factor 10 difference). Therefore, this oxidation phenomenon seems to be driven by the water impurity in the atmosphere which is very low in our case.

**EXAFS-XANES Study of Stoichiometric and Substoichiometric MOX.** To obtain more details on uranium and plutonium oxidation state and local structure in the two MOX samples, EXAFS and XANES measurements have been performed. The samples used for these analyses came from the same pellets as those used in the first part of this study, with a one year delay after the original sintering. Spontaneous oxidation described above or $\alpha$ self-irradiation would be responsible for the evolution of the MOX structure. To achieve a rigorous comparison between long-range ordering from XRD and local structure from EXAFS, the XRD measurements were repeated at the same time as the EXAFS study, i.e., one year after pellet sintering and one month after crushing the samples (Figure 7). In the case of $U_{0.7}Pu_{0.3}O_{2.00}$ a lattice parameter increase of 0.08% is observed (5.4531(9) Å), and is attributed to $\alpha$ self-irradiation. Kato et al.[30] proposed a general formula to determine lattice expansion in MOX:

$$\Delta a/a_0 = A(1 - \exp(B\lambda' t)) \quad (2)$$

with $A = 2.9 \times 10^{-3}$ and $B = -12\,000$.

The effective decay constant $\lambda'$ takes into account the specific decay constant of each isotope and their molar fraction in MOX (Table 1). For our material, the value of $\lambda' = 2.8 \times 10^{-12}$ $s^{-1}$ (for the calculation details, see the Kato's study[30]). The lattice expansion after one year in our study is in good agreement with this formula, which also gives 0.08% after one year of self-irradiation. Though significant, it is far from the saturation value of 0.29%.

The substoichiometric MOX $U_{0.7}Pu_{0.3}O_{2-x}$ still exhibits its biphasic composition one year after sintering. Due to $\alpha$ self-irradiation, eq 1 cannot be applied directly to deduce the O/M from the lattice parameters and phase proportion. Nevertheless, if one considers that $\alpha$ irradiation has the same impact on lattice parameter expansion for stoichiometric and substoichiometric MOX, the lattice parameter can be corrected. On the



DOI: 10.1021/acs.inorgchem.5b00392
*Inorg. Chem.* 2015, 54, 5358−5365

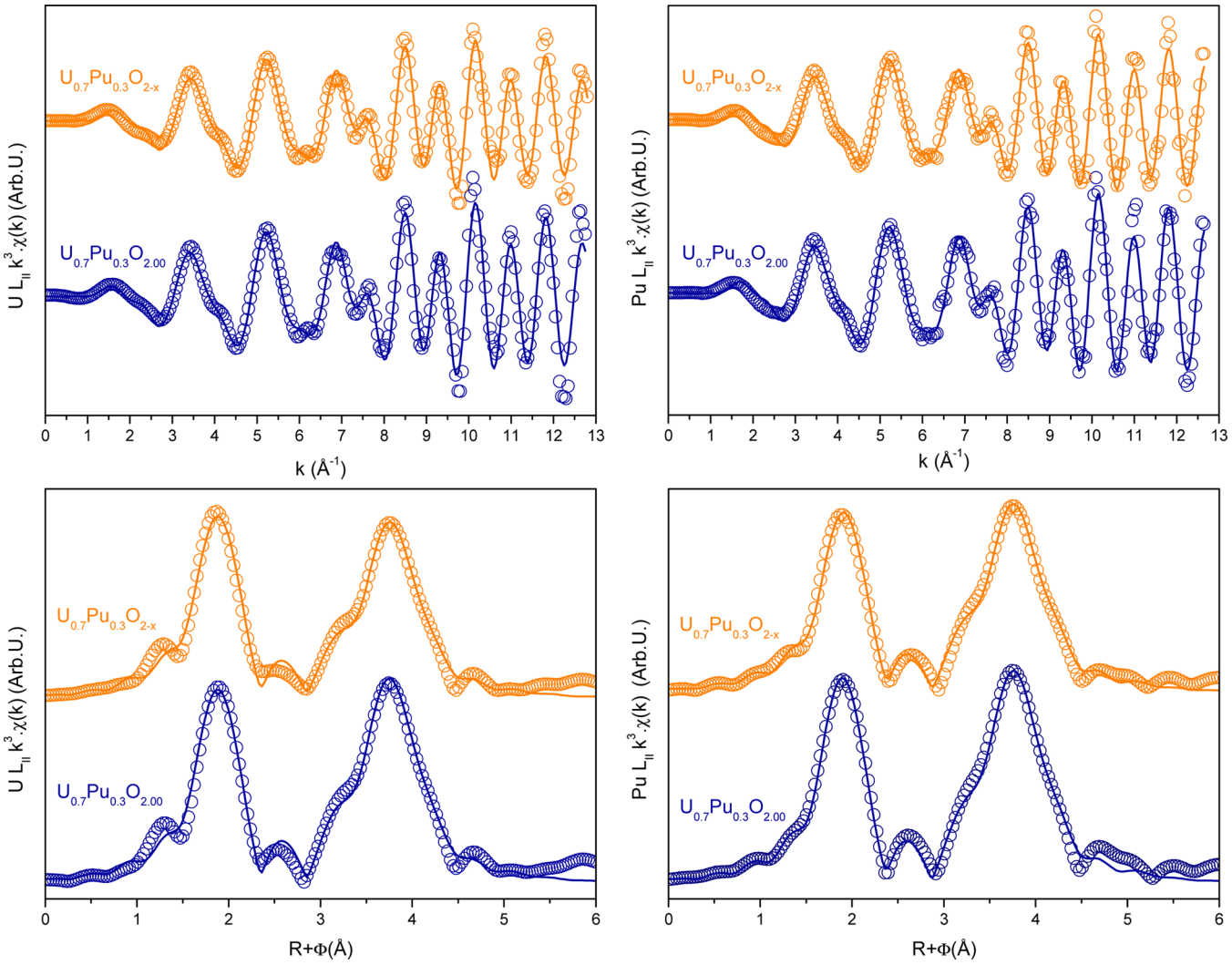


**Figure 9.** Experimental and fitted EXAFS spectra at Pu-$L_{II}$ and U-$L_{II}$ edges (top) and the respective Fourier transforms (bottom). Circles correspond to the experimental data and lines to the fitted data.

**Table 3. Structural Distances Extracted from Fit of EXAFS Spectra Measured at Both U-$L_{II}$ and Pu-$L_{II}$ Edges**

| sample | edge | shell | $N$ | $R$ [Å] | $\sigma^2$ [Å$^2$] |
|---|---|---|---|---|---|
| $U_{0.7}Pu_{0.3}O_{2.00}$ | U-$L_{II}$ | O | 7.7(5) | 2.349(5) | 0.006(1) |
| | | M | 12.3(5) | 3.86(1) | 0.005(1) |
| | | O | 26(2) | 4.51(1) | 0.010(1) |
| | Pu-$L_{II}$ | O | 8.5(5) | 2.351(5) | 0.007(1) |
| | | M | 11.6(5) | 3.86(1) | 0.004(1) |
| | | O | 24(2) | 4.51(1) | 0.008(1) |
| $U_{0.7}Pu_{0.3}O_{2-x}$ | U-$L_{II}$ | O | 7.5(5) | 2.348(5) | 0.006(1) |
| | | M | 11.8(5) | 3.86(1) | 0.006(1) |
| | | O | 23(2) | 4.51(1) | 0.010(1) |
| | Pu-$L_{II}$ | O | 7.9(5) | 2.359(5) | 0.007(1) |
| | | M | 11.4(5) | 3.86(1) | 0.005(1) |
| | | O | 24(2) | 4.50(1) | 0.009(1) |

**Table 4. Crystallographic Distances Deduced from Lattice Parameters**

| sample | atom 1 | atom 2 | $N$ | $d_{1-2}$ [Å] | $a$ [Å] |
|---|---|---|---|---|---|
| $U_{0.7}Pu_{0.3}O_{2.00}$ | U−Pu | O | 8 | 2.361 | |
| | | U−Pu | 12 | 3.856 | 5.4531(9) |
| | | O | 24 | 4.522 | |
| $U_{0.7}Pu_{0.3}O_{2-x}$ | U−Pu | O | 8 | 2.364 | |
| 79(5)% | | U−Pu | 12 | 3.860 | 5.4591(9) |
| | | O | 24 | 4.526 | |
| $U_{0.7}Pu_{0.3}O_{2-x}$ | U−Pu | O | 8 | 2.369 | |
| 21(5)% | | U−Pu | 12 | 3.868 | 5.4701(9) |
| | | O | 24 | 4.536 | |

basis of this approach, the overall calculated composition is $U_{0.7}Pu_{0.3}O_{1.971\pm0.010}$.

The XANES data are presented in Figure 8 and give information on uranium and plutonium oxidation states. In the case of uranium, the very good superposition of $U_{0.7}Pu_{0.3}O_{2.00}$ and $U_{0.7}Pu_{0.3}O_{2-x}$ with the $UO_2$ reference spectrum indicates that only uranium(IV) is present in both MOX samples. It has been shown previously that a shift is clearly observed in a case of slightly hyperstoichiometric MOX $U_{0.7}Pu_{0.3}O_{2+x}$ due to the U(IV)−U(V) mixture[6] which is definitely not the case here. Furthermore, the Pu-$L_{III}$ absorption edge of stoichiometric MOX shows a good superposition with that of the $PuO_2$ reference, confirming the tetravalent oxidation state of Pu and in turn the stoichiometric oxygen composition $U_{0.7}Pu_{0.3}O_{2.00}$. In contrast, the substoichiometric sample shows a shift of the signal to lower energy indicative of the presence of a lower redox state. From a linear combination fit with Pu(III) and



DOI: 10.1021/acs.inorgchem.5b00392
*Inorg. Chem.* 2015, 54, 5358−5365

Pu(IV) references, a composition of $U_{0.7}Pu_{0.3}O_{1.978\pm0.010}$ is derived (Table 2), in good agreement with that derived from XRD.

The EXAFS data and corresponding Fourier transforms are given in Figure 9. The local environments around uranium and plutonium in stoichiometric MOX $U_{0.7}Pu_{0.3}O_{2.00}$ (Table 3), as deduced from EXAFS shell fitting, agree well with the long-range structure derived from the crystallographic data (Table 4). Thus, we found no evidence for a significant local ordering around individual actinides, corroborating with solid solution ideality. Surprisingly, even at the first oxygen shell, no significant differences between U−O and Pu−O distances were observed, in contrast to the pure oxides ($d_{U-O}$ = 2.370(5) Å in $UO_2$ and $d_{Pu-O}$ = 2.333(5) Å in $PuO_2$[6]). Similar behavior was observed in $U_{0.5}Pu_{0.5}O_{2.00}$,[6] suggesting a contraction of U−O and an elongation of Pu−O bond distances in stoichiometric MOX compared to pure oxides. These results contrast those reported for $ThO_{2.00}$ solid solutions with $MO_{2.00}$ (M = U, Pu,[31] or Am[32]), where metal−oxygen lengths do not exhibit strong variation between pure oxides and solid solutions.

For substoichiometric $U_{0.7}Pu_{0.3}O_{2-x}$, the results are nearly the same as for the stoichiometric compound, showing no significant change of the uranium and plutonium local environments. As the EXAFS signal represents the statistically weighted average of the Pu and U atoms present in the sample, the fit values are an average of local environments in both phases present in this material. A very slight increase of plutonium−oxygen distance seems to occur, which would be consistent with the presence of Pu(III) in $U_{0.7}Pu_{0.3}O_{2-x}$ as suggested by XANES, but a significant observation of this phenomenon would probably require a stronger deviation from stoichiometry.

## CONCLUSION

A detailed structural investigation has been performed on two MOX samples with 30% Pu content. The solid solution ideality has been demonstrated definitively in stoichiometric $U_{0.7}Pu_{0.3}O_{2.00}$, using a combination of XRD, XAS, and $^{17}O$ MAS NMR. The latter clearly determines the random distribution of uranium and plutonium in the network. The use of the $^{17}O$ MAS NMR technique opens new routes for the investigation of cationic distribution into radioactive materials which contain elements of similar atomic number.

As expected for substoichiometric $U_{0.7}Pu_{0.3}O_{2-x}$, a biphasic composition of the material was found. This study provides a new illustration of $U_{0.7}Pu_{0.3}O_{2-x}$ sensitivity toward oxidation but with a significantly slower rate compared to previous data, leading us to the conclusion that this oxidation phenomenon seems to be mainly driven by water impurities in the atmosphere.

Finally, an EXAFS-XANES study of the two MOX samples has been performed. XANES confirms the presence of Pu(III) in $U_{0.7}Pu_{0.3}O_{2-x}$ and more generally the O/M in the two materials. EXAFS shows the close similarity between the long-range ordering of the material and the local structure around uranium and plutonium.

## AUTHOR INFORMATION

### Corresponding Author

*E-mail: jean-francois.vigier@ec.europa.eu.

### Notes

The authors declare no competing financial interest.

## ACKNOWLEDGMENTS

We are thankful to Daniel Bouexière for XRD analysis and to Sébastien Gardeur, Co Boshoven, and Chris Selfslag for their help during the sample preparation. We would like also to thank Randolf Butzbach, Patrick Colomp, and Andrea Cambriani for their help during transport organization and their assistance at the beamline.

## REFERENCES

(1) Sarotto, M.; Castelliti, D.; Fernandez, R.; Lamberts, D.; Malambu, E.; Stankovskiy, A.; Jaeger, W.; Ottolini, M.; Martin-Fuertes, F.; Sabathé, L.; Mansani, L.; Baeten, P. *Nucl. Eng. Des.* **2013**, *265*, 184−200.

(2) Vaudez, S.; Belin, R. C.; Aufore, L.; Sornay, P.; Grandjean, S. *J. Nucl. Mater.* **2013**, *442*, 227−234.

(3) Philipponneau, Y. *J. Nucl. Mater.* **1992**, *188*, 194−197.

(4) Vauchy, R.; Robisson, A.-C.; Audubert, F.; Hodaj, F. *Ceram. Int.* **2014**, *40*, 10991−10999.

(5) Sari, C.; Benedict, U.; Blank, H. *J. Nucl. Mater.* **1970**, *35*, 267−277.

(6) Martin, P.; Grandjean, S.; Valot, C.; Carlot, G.; Ripert, M.; Blanc, P.; Hennig, C. *J. Alloys Compd.* **2007**, *444−445*, 410−414.

(7) Vauchy, R. Étude du rapport O/M dans des nouveaux combustibles oxydes à base d'U et Pu: élaboration et caractérisation de matériaux modèles $U_{1-y}Pu_yO_{2-x}$. Ph.D. Thesis, Université de Grenoble, 2014.

(8) Böhler, R.; Welland, M. J.; Prieur, D.; Cakir, P.; Vitova, T.; Pruessmann, T.; Pidchenko, I.; Hennig, C.; Guéneau, C.; Konings, R. J. M.; Manara, D. *J. Nucl. Mater.* **2014**, *448*, 330−339.

(9) Sood, D. D. *J. Sol-Gel Sci. Technol.* **2011**, *59*, 404−416.

(10) Kato, M.; Takeuchi, K.; Uchida, T.; Sunaoshi, T.; Konashi, K. *J. Nucl. Mater.* **2011**, *414*, 120−125.

(11) Petříček, V.; Dušek, M.; Palatinus, L. *Z. Kristallogr.* **2014**, *229*, 345−352.

(12) Martel, L.; Somers, J.; Berkmann, C.; Koepp, F.; Rothermel, A.; Pauvert, O.; Selfslag, C.; Farnan, I. *Rev. Sci. Instrum.* **2013**, *84*, 055112.

(13) Massiot, D.; Fayon, F.; Capron, M.; King, I.; Le Calvé, S.; Alonso, B.; Durand, J.-O.; Bujoli, B.; Gan, Z.; Hoatson, G. *Magn. Reson. Chem.* **2002**, *40*, 70−76.

(14) Matz, W.; Schell, N.; Bernhard, G.; Prokert, F.; Reich, T.; Claussner, J.; Oehme, W.; Schlenk, R.; Dienel, S.; Funke, H.; Eichhorn, F.; Betzl, M.; Prohl, D.; Strauch, U.; Huttig, G.; Krug, H.; Neumann, W.; Brendler, V.; Reichel, P.; Denecke, M. A.; Nitsche, H. *J. Synchrotron Radiat.* **1999**, *6*, 1076−1085.

(15) Desgranges, L.; Baldinozzi, G.; Rousseau, G.; Nièpce, J.-C.; Calvarin, G. *Inorg. Chem.* **2009**, *48*, 7585−7592.

(16) Prieur, D.; Carvajal-Nunez, U.; Vitova, T.; Somers, J. *Eur. J. Inorg. Chem.* **2013**, *2013*, 1518−1524.

(17) Ravel, B.; Newville, M. *J. Synchrotron Radiat.* **2005**, *12*, 537−541.

(18) Martin, P.; Ripert, M.; Petit, T.; Reich, T.; Hennig, C.; D'Acapito, F.; Hazemann, J. L.; Proux, O. *J. Nucl. Mater.* **2003**, *312*, 103−110.

(19) Prieur, D.; Martin, P. M.; Jankowiak, A.; Gavilan, E.; Scheinost, A. C.; Herlet, N.; Dehaudt, P.; Blanchart, P. *Inorg. Chem.* **2011**, *50*, 12437−12445.

(20) Prieur, D.; Martin, P. M.; Lebreton, F.; Delahaye, T.; Jankowiak, A.; Laval, J. P.; Scheinost, A. C.; Dehaudt, P.; Blanchart, P. *J. Solid State Chem.* **2012**, *194*, 206−211.

(21) Prieur, D.; Vigier, J.-F.; Wiss, T.; Janssen, A.; Rothe, J.; Cambriani, A.; Somers, J. *J. Solid State Chem.* **2014**, *212*, 7−12.

(22) Kato, M.; Konashi, K. *J. Nucl. Mater.* **2009**, *385*, 117−121.

(23) Martel, L.; Vigier, J.-F.; Prieur, D.; Nourry, S.; Guiot, A.; Dardenne, K.; Boshoven, J.; Somers, J. *J. Phys. Chem. C* **2014**, *118*, 27640−27647.

(24) Düvel, A.; Ruprecht, B.; Heitjans, P.; Wilkening, M. *J. Phys. Chem. C* **2011**, *115*, 23784−23789.



DOI: 10.1021/acs.inorgchem.5b00392
*Inorg. Chem.* 2015, 54, 5358−5365

(25) Martel, L.; Magnani, N.; Vigier, J.-F.; Boshoven, J.; Selfslag, C.; Farnan, I.; Griveau, J.-C.; Somers, J.; Fanghänel, T. *Inorg. Chem.* **2014**, *53*, 6928−6933.
(26) Truphémus, T.; Belin, R. C.; Richaud, J.-C.; Reynaud, M.; Martinez, M.-A.; Félines, I.; Arredondo, A.; Miard, A.; Dubois, T.; Adenot, F.; Rogez, J. *J. Nucl. Mater.* **2013**, *432*, 378−387.
(27) Vauchy, R.; Belin, R. C.; Robisson, A.-C.; Hodaj, F. *J. Eur. Ceram. Soc.* **2014**, *34*, 2543−2551.
(28) Guéneau, C.; Dupin, N.; Sundman, B.; Martial, C.; Dumas, J.-C.; Gossé, S.; Chatain, S.; Bruycker, F. D.; Manara, D.; Konings, R. J. M. *J. Nucl. Mater.* **2011**, *419*, 145−167.
(29) Duriez, C.; Alessandri, J.-P.; Gervais, T.; Philipponneau, Y. *J. Nucl. Mater.* **2000**, *277*, 143−158.
(30) Kato, M.; Komeno, A.; Uno, H.; Sugata, H.; Nakae, N.; Konashi, K.; Kashimura, M. *J. Nucl. Mater.* **2009**, *393*, 134−140.
(31) Hubert, S.; Purans, J.; Heisbourg, G.; Moisy, P.; Dacheux, N. *Inorg. Chem.* **2006**, *45*, 3887−3894.
(32) Carvajal-Nunez, U.; Prieur, D.; Vitova, T.; Somers, J. *Inorg. Chem.* **2012**, *51*, 11762−11768.



DOI: 10.1021/acs.inorgchem.5b00392
*Inorg. Chem.* 2015, 54, 5358−5365